Optik - International Journal for Light and Electron Optics 267 (2022) 169643

Contents lists available at ScienceDirect

Optik

journal homepage: www.elsevier.com/locate/ijleo

Transmission factors, mechanical, and gamma ray attenuation properties of barium-phosphate-tungsten glasses: Incorporation impact of WO_3

H.O. Tekin [a,b,*], Ghada ALMisned [c], Y.S. Rammah [d,**,1], Emad M. Ahmed [e], Fatema T. Ali [f], Duygu Sen Baykal [g], Wiam Elshami [a], Hesham M.H. Zakaly [h,j], Shams A.M. Issa [i,j], G. Kilic [k], Antoaneta Ene [l,**,2]

[a] Department of Medical Diagnostic Imaging, College of Health Sciences, University of Sharjah, 27272 Sharjah, United Arab Emirates
[b] Istinye University, Faculty of Engineering and Natural Sciences, Computer Engineering Department, Istanbul 34396, Turkey
[c] Department of Physics, College of Science, Princess Nourah Bint Abdulrahman University, P.O. Box 84428, Riyadh 11671, Saudi Arabia
[d] Department of Physics, Faculty of Science, Menoufia University, Shebin El-Koom, 32511 Menoufia, Egypt
[e] Department of Physics, College of Science, Taif University, P.O. Box 11099, Taif 21944, Saudi Arabia
[f] Center for Advanced Materials Research, Research Institute of Sciences and Engineering, University of Sharjah, Sharjah 27272, United Arab Emirates
[g] Istanbul Kent University, Vocational School of Health Sciences, Medical Imaging Techniques, Istanbul 34433, Turkey
[h] Institute of Physics and Technology, Ural Federal University, 620002 Ekaterinburg Russia
[i] Physics Department, Faculty of Science, University of Tabuk, Tabuk 47512, Saudi Arabia
[j] Physics Department, Faculty of Science, Al-Azhar University, Assiut 71524, Egypt
[k] Eskisehir Osmangazi University, Faculty of Science and Letters, Department of Physics, Eskisehir, Turkey
[l] INPOLDE Research Center, Department of Chemistry, Physics and Environment, Faculty of Sciences and Environment, Dunarea de Jos University of Galati, 47 Domneasca Street, 800008 Galati, Romania

ARTICLE INFO

Keywords:
BaO- P_2O_5- WO_3 glass system
Mechanical properties
Radiation shielding
MCNPX

ABSTRACT

The purpose of this study is to conduct a thorough examination of the direct and indirect impacts of increasing the quantity of heavy WO_3 on gamma-ray transmission, shielding and mechanical properties for some selected barium-phosphate-tungsten glasses. Accordingly, mechanical properties of barium-phosphate-tungsten oxides with chemical formula (50-x)P_2O_5-50BaO-xWO_3 (x = 0.0(S1), 5.0(S2), 10(S3), and 15(S4)) mol% was evaluated using Makishima-Mackenzie model. Next, newly online Phy-X/PSD software and Monte Carlo code were used to examine the gamma radiation characteristics. Gamma-ray transmission factor (TF) values were calculated for S1, S2, S3 and, S4 glass samples for a range of well-known radioisotope energies such for ^{67}Ga, ^{57}Co-57, ^{111}In-111, ^{133}Ba, ^{201}Tl, $^{99\ m}$Tc, ^{51}Cr, ^{131}I, ^{58}Co, ^{137}Cs, ^{60}Co. The total packing density (V_t) was enhanced from 0.589 for S1 glass sample (free with WO_3) to 0.605 for S4 glass sample (with highest WO_3 =15 mol%). The total energy dissociation (G_t) of the investigated glasses was increased with increasing the WO_3 content: from 51.7 (kJ/cm^3) for S1 glasses to 52.45 (kJ/cm^3)

* Corresponding author at: Department of Medical Diagnostic Imaging, College of Health Sciences, University of Sharjah, 27272 Sharjah, United Arab Emirates.
** Corresponding authors.
E-mail addresses: tekin765@gmail.com (H.O. Tekin), dr_yasser1974@yahoo.com (Y.S. Rammah), Antoaneta.Ene@ugal.ro (A. Ene).

[1] The researcher (Y.S. Rammah) is funded by a full scholarship (2019/2020) from the Ministry of Higher Education of the Arabic Republic of Egypt.
[2] The work of Antoaneta Ene and the APC were supported by Dunarea de Jos University of Galati, Romania through the grant no. RF 3621/2021.

https://doi.org/10.1016/j.ijleo.2022.169643
Received 2 June 2022; Accepted 11 July 2022
Available online 13 July 2022

for S4 glasses. All mechanical moduli were improved with increasing the tungsten trioxide concentration in the studied glasses. Poisson's ratios were increased with increasing the WO_3 concentration. The trend of linear (LAC) and mass attenuation (MAC) coefficients were followed as: $(LAC, MAC)_{S1} < (LAC, MAC)_{S2} < (LAC, MAC)_{S3} < (LAC, MAC)_{S4}$. Half (HVL) and tenth (TVL) value layers have the trend as $(HVL, TVL)_{S1} > (HVL, TVL)_{S2} > (HVL, TVL)_{S3} > (HVL, TVL)_{S4}$. The effective atomic number (Z_{eff}) and electron density (N_{eff}) have the same trend. The lowest transmission Factor (TF) values for all glass specimens were examined at a thickness of 3 cm. Furthermore, the S4 sample displayed the least transmission tendency across all glass thicknesses evaluated.

1. Introduction

The application of ionizing radiation has risen dramatically in recent years, particularly in the medical and pharmaceutical industries. Considering ionizing radiation increases cancer risk, it is essential to practice radiation protection in all settings that employ radiation. For this purpose, the ALARA (As Low As Reasonably Achievable) principle was established. The three pillars of this radiation protection strategy are limiting exposure duration, increasing distance from the radiation source, and utilizing shielding to reduce the scatter radiation [1]. In many applications, the duration of exposure and distance cannot be manipulated as they affect the purpose of the radiation procedure. Therefore, shielding can be used and formulated in different formats, including concreate, garments, and glass. Concrete is a time-honored means of radiation shielding. It is available in various forms and sizes and has a reasonable price. Nonetheless, it has some drawbacks, including high thickness, opaqueness, the possibility of cracks resulting from excessive radiation exposure, and a gradual loss of density and mechanical strength over time [2]. While garments, aprons and gloves provide radiation protection, they are delicate structures prone to rip and interfere with radiation protective processes [3]. Glass shields are an excellent choice for radiation shielding due to their low cost and ease of fabrication. Nonetheless, it is unclear, has a low strength, and poses toxicity concerns [4]. The determinant of the quality of shielding materials is atomic number, density, and composition. In addition, the construction of shields varies by manufacturer, and the metal content and rubber quality affect their flexibility, durability, radiation absorption effectiveness, and weight [5]. As a result, there is a surge of attention in developing innovative shielding materials to overcome drawbacks of the available shielding materials and increase the efficiency of radiation protection [6–9]. Recently, several scientists have focused their attention to glass systems as radiation shielding materials. The major radiation shielding parameters such as mass and linear attenuation coefficients (MAC and LAC), half value layer (HVL), tenth value layer (TVL), mean free path (MFP), effective atomic number (Z_{eff}), exposure (EBF) and energy absorption buildup (EABF) factors are evaluated for several suggested shielding materials [7–24]. Monte Carlo simulation techniques MCNPX [25] as well as theoretically using Phy-X/PSD program [26] were used to determine the mass attenuation coefficient (μ/ρ) numerically [27–30]. In the current study, the direct influence of tungsten trioxide (WO_3) on mechanical and radiation shielding properties of barium phosphate ($BaO/ P_2O_5/ WO_3$) glass system was investigated.

2. Materials and methods

2.1. Studied glasses

Four glasses of barium-phosphate-tungsten oxides with chemical formula $(50\text{-}x)P_2O_5\text{-}50BaO\text{-}xWO_3$ (x = 0, 5, 10, and 15 mol%) were selected from previous work [31]. All details along with the chemical composition of the studied glasses are collected in Table 1.

2.2. Mechanical properties of the studied glasses

Mechanical properties (elastic moduli and Poisson's ratio) of the studied $BaO\text{-}P_2O_5\text{-}WO_3$ glasses (S1-S4) were examined via the conventional model (Makishima-Mackenzie) [32–36]. It is well known that the elastic moduli is the function of both packing density (V_t) and the dissociation energy per unit volume (G_t) of the chemical bonds in the glass as [32–36]:

$$V_t = \left(\frac{1}{V_m}\right)\sum_i (V_i x_i) \quad (1)$$

Table 1
Samples code, chemical composition, density, and molar volume of $(50\text{-}x)P_2O_5\text{-}50BaO\text{-}xWO_3$ (x = 0.0, 5.0, 10, and 15 mol% glasses.

Samples Code	Composition (mol%)			Density, ρ (g/cm^3)[27]	Molar volume, V_m (cm^3/mol)[27]
	BaO	**P_2O_5**	**WO_3**		
S1	50	50	0.0	3.64	40.6
S2	50	45	5.0	3.87	39.3
S3	50	40	10	4.21	37.2
S4	50	35	15	4.45	36.2

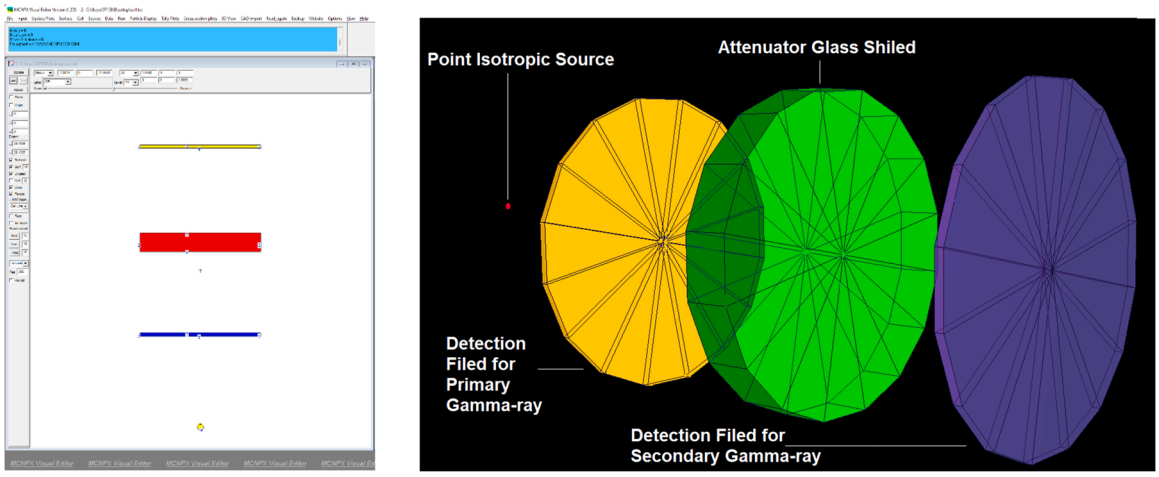

Fig. 1. (a) 2-D view of designed MCNPX simulation setup **(b)** 3-D illustration of designed MCNPX setup (2-D and 3-D views are obtained from MCNPX Visual Editor VisedX22S).

$$G_t = \sum_i (G_i x_i) \quad \left(kJ/cm^3\right) \tag{2}$$

Where, (V_i) is the ionic radius and (G_i) is the average strength of each oxide in the glassy system. The Young`s (E^{MM}), bulk (K^{MM}), shear (S^{MM}), and longitudinal (L^{MM}) moduli can be evaluated in GPa unit as in the nest relations (3–6) [32–36]:

$$E^{MM} = 2V_t G_t \tag{3}$$

$$K^{MM} = 1.2V_t E^{MM} \tag{4}$$

$$S^{MM} = \frac{\left(3E^{MM}K^{MM}\right)}{\left(9K^{MM} - E^{MM}\right)} \tag{5}$$

$$L^{MM} = K^{MM} + \frac{4}{3}S^{MM} \tag{6}$$

In addition, Poisson's ratio (σ_{MM}) can be calculated via:

$$\sigma^{MM} = \left(\frac{E^{MM}}{2G^{MM}}\right) - 1 \tag{7}$$

2.3. Monte Carlo simulation phase for transmission factors (TFs)

It is well recognized that structural adjustments to materials influence the reduction rates of energetic photons. These changes may be studied using parameters or computed by performing an assessment on the whole material. The Transmission Factor [37] is defined as the ratio of the input radiation intensity to the output radiation, also known as secondary radiation, produced by the material as a consequence of attenuation. In this study, we determined the TFs of the studied glasses for a range of well-known radioisotope energies such ^{67}Ga, ^{57}Co-57, ^{111}In-111, ^{133}Ba, ^{201}Tl, $^{99\,m}$Tc, ^{51}Cr, ^{131}I, ^{58}Co, ^{137}Cs, ^{60}Co using the MCNPX [25] general-purpose Monte Carlo simulation code (Version 2.7.0). Two detecting zones are defined in front and behind the glass shield to obtain primary and secondary gamma radiation intensities. The MCNPX simulation setup for estimating the gamma-ray transmission factor is shown in Fig. 1. Throughout the Monte Carlo simulation codes, the procedure begins with the creation of an acceptable input file that contains the features of the complete simulation environment in which the research will be conducted. In this study, a basic input file was prepared to provide cell, surface and data cards and visualized as in Fig. 1. The prepared input file's two primary deciding criteria are the elemental percentage distributions and densities specified for each glass sample. Additionally, by specifying the energy values of the aforementioned radioisotopes for each simulation cycle, it was possible to assess the transmission factor as a function of energy, as described in the following sections. We used Lenovo® ThinkStation-P620/30E0008QUS Workstation during the Monte Carlo simulation phases.

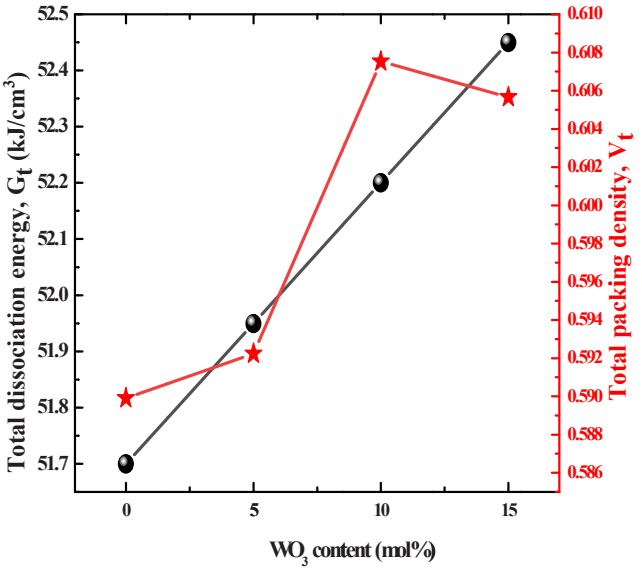

Fig. 2. : Variation of G_t and V_t as a function of WO_3 content (mol%) of the investigated glasses.

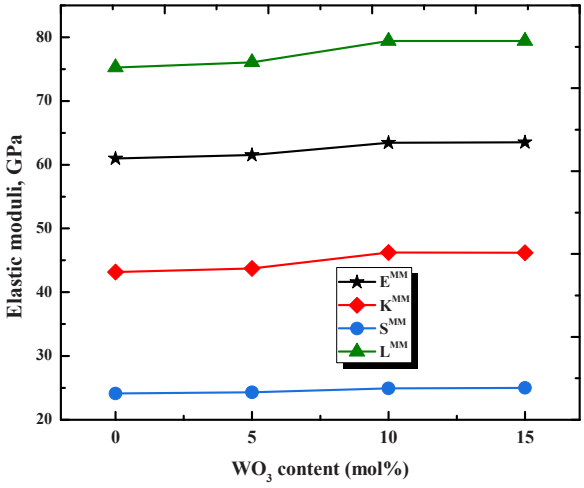

Fig. 3. : Variation of elastic moduli as a function of WO_3 content mol% of the investigated glasses.

3. Results and discussions

3.1. Mechanical properties

By raising the WO3 concentration in the glass network, the network's structural configuration changes dramatically; this shift may be due to a reduction in the bond length or interatomic gap between the glass network's atoms, which results in structure compaction [31]. Numerous tungstate compounds, notably W2O3$(PO_4)_2$ (which is also a member of the BaO-WO_3-P_2O_5 system), form WO_6 octahedra [38,39]. Each WO_6 octahedron in this combination is connected by corner sharing to four PO4 tetrahedra, with one corner shared with another WO_6 octahedron and one oxygen atom remaining unshared [31]. In the molecule W_2O_3 $(PO_4)_2$, it is capable of forming terminal W═O bonds. In the studied BaO-WO_3-P_2O_5 glasses, the presence of Ba^{2+} compensating ions resulted in the existence of non-bridging oxygen atoms in P-O or W-O links [31]. The total packing density (V_t) was calculated via Eq. (1) and the total dissociation energy (G_t) was calculated via Eq. (2) for all studied glasses (S1-S4). The mentioned step was achieved using the (V_i) and (G_i) values of the glass system oxides BaO, P_2O_5, and WO_3. Fig. 2 displays the variation of G_t and V_t as a function of tungsten trioxide (WO_3) in mole% of the studied glasses (S1-S4). The (V_t) was increased in from 0.589 for sample free with WO_3 (S1) to 0.605 for sample rich with WO_3 (S4) as shown in Fig. 2. This trend can be related to the increasing content of WO_3 at the expense of P_2O_5, is energizing the glass structure. The bonds P-O with lower energy strength 599.1 ± 12.6 (kJ/mole [40]) are replaced by W-O bonds of higher

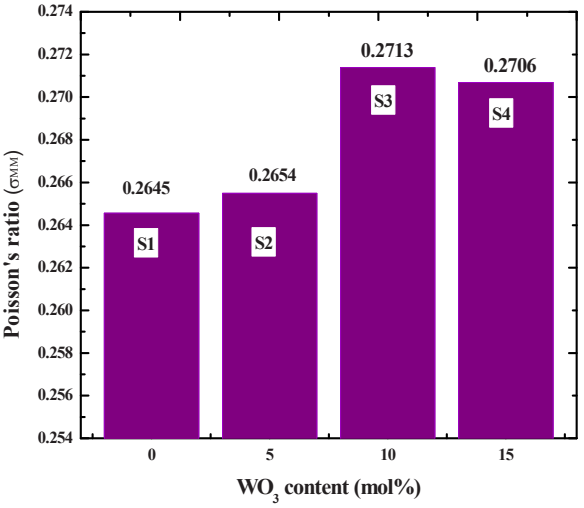

Fig. 4. : Variation of Poisson's ratio as a function of WO_3 content (mol%) of the investigated glasses.

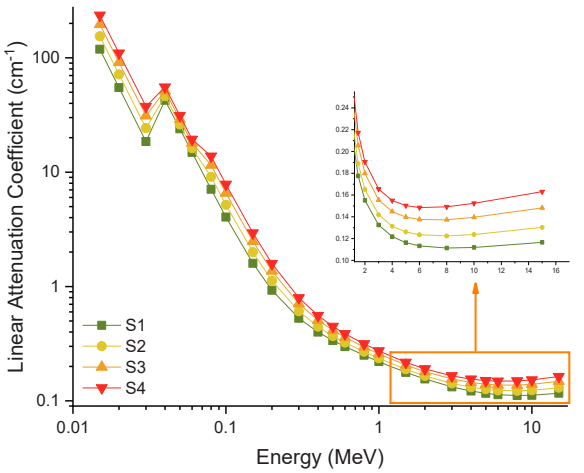

Fig. 5. : Variations of linear attenuation coefficient (cm^{-1}) with photon energy (MeV) for all S1-S4 glasses.

energy strength 672.0 ± 20.9 (kJ/mole [40]) in the glass structural network. As well, the total packing density V_t of the studied system increases with WO_3. Although the packing density of the increasingly forming WO_6 is lower than that of PO_4, 2.13 and 3.46 × 10^{-5} m^3/mol, respectively. This behavior could be correlated with the decreasing molar volume V_m of the glass system P_2O_5-BaO-WO_3 [31]. From Figure, with increasing the content of WO_3 than 10 mol% in the studied glass network, the total packing density (V_t) starts to somewhat decrease, this may be attributed to with increasing WO_3 than that value, the peak of the greatest band for W-O bond vibrations moves to a lower wavenumber, as previously shown by Raman and ^{31}P NMR. spectroscopies of the studied glasses [31]. In addition, the insertion of WO_3 at the expense of P_2O_5 increases the total dissociation energy (G_t). The WO_3 forms predominantly in octahedral WO_6 units [40], that have much higher dissociation energy than that of tetrahedron PO_4, 6.78 and 2.82 × 10^{10} J/m^3, respectively [41]. Thus, the substitution of WO_6 in place of tetrahedron PO_4 is gaining G_t of the system P_2O_5-BaO-WO_3. Moreover, the WO_3 has higher dissociation energy (67.8 kJ/cm^3) compared to that of BaO (40.6 kJ/cm^3) and P_2O_5 (62.8 kJ/cm^3) [29]. Young's modulus describes a material's ability to deform under the influence of applied stress. It is higher as the sudden strain is minimal [42]. By applying the (V_t) and (G_t) values in relation (3), Young`s elastic (E^{MM}) modulus can be calculated for all studied glasses (S1-S4). The trend of the (E^{MM}) is collected in and drawn in Fig. 3. One can observe that the values of the (E^{MM}) were increased with enhancement of tungsten trioxide (WO_3) content in glasses; the (E^{MM}) values were changed from 60.99581Gpa for sample S1 to 63.53405 GPa for sample S4. Using relation (4) with applying the values of (E^{MM}), the values of the bulk (K^{MM}) modulus of S1-S4 glasses were obtained. Values were increased from 43.17782 GPa for sample S1 to 46.17626 GPa for sample S4. Also, by using relations 5 and 6, shear (S^{MM}) and longitudinal (L^{MM}) elastic moduli were computed, respectively and graphed in Fig. 3. Values of the (S_{MM}) were increased from 24.11749 GPa to 24.99996 GPa, while values of the (L_{MM}) was increased from 75.25408 GPa to 79.42621 GPa. As seen in Fig. 3, the elastic moduli tend to rise as the network grows from a two-dimensional structure formed of PO_4 chains randomly dispersed within the

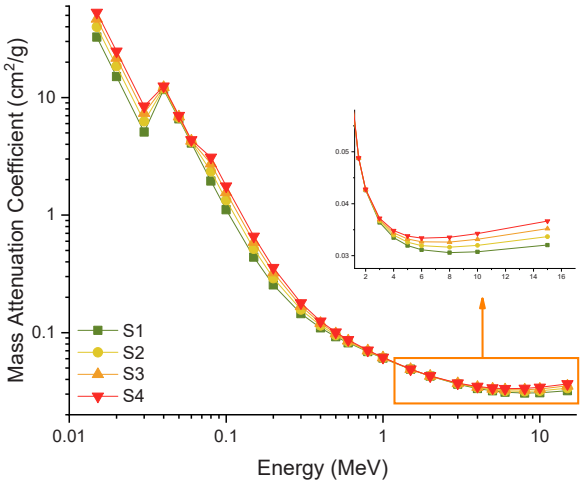

Fig. 6. Variation of mass attenuation coefficients (cm^2/g) with photon energy (MeV) for all S1-S4 glasses.

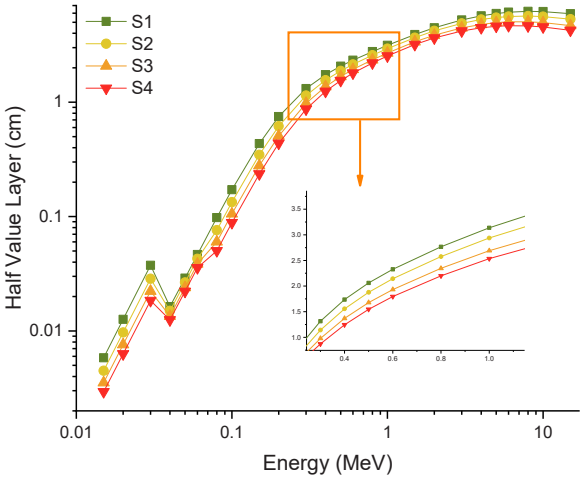

Fig. 7. Variation of half value layer (cm) with photon energy (MeV) for all S1-S4 glasses.

P_2O_5 in glasses devoid of WO_3 to a more strongly cross-linked compact structure in glasses enriched with WO_3. The increase in elastic moduli is more pronounced when the WO_3 content is more than 5%, indicating that the insertion of additional WO6 units improves network connection and crosslink density [42]. The Poisson's ratio (MM) of the analyzed glasses was determined using relation (7). As seen in Fig. 4, the value of (σ^{MM}) raised from 0.2645 for S1 glasses to 0.2706 for S4 glasses. The Poisson's ratio values found for the examined glasses were consistent with the notion that the Poisson's ratio is approximately invariant and close to 0.252. According to T. Rouxel [43], Poisson's ratio may be indicative of the vitreous network's structural structure. Poisson's ratio, on the other hand, is equivalent to 0.4, 0.25, or 0.15 for a glassy network with connectivity of one, two, or three. As a result, one may deduce that the addition of WO_3 retains the examined material's two-dimensional structure [40]. Our results corroborate previous research on the propagation of ultrasonic waves in tellurium glasses [44,45], which shown that increasing the concentration of WO_3 in glasses improves elastic moduli. Fig. 6.

3.2. Radiation shielding characteristics

In addition to extensive mechanical properties, gamma-ray shielding properties of S1-S4 glasses have been studied in a wide photon energy range (i.e., from 0.015 MeV to 15 MeV). For the glasses examined, it is worthy to state a considerable rise in densities between the S1 and S4 samples owing to the varied WO_3 additive rates. An important factor contributing to the rise is that the heavy atom contribution rate has been steadily increasing in the S1 sample. S4 sample's highest density was 4.45 g/cm^3, a consequence of the most significant WO_3 additive's influence. Linear Attenuation coefficient (μ) may be used to describe an essential characteristic that is based on material density and can be studied for each energy value. To illustrate how attenuation changes with increasing energy, Fig. 5

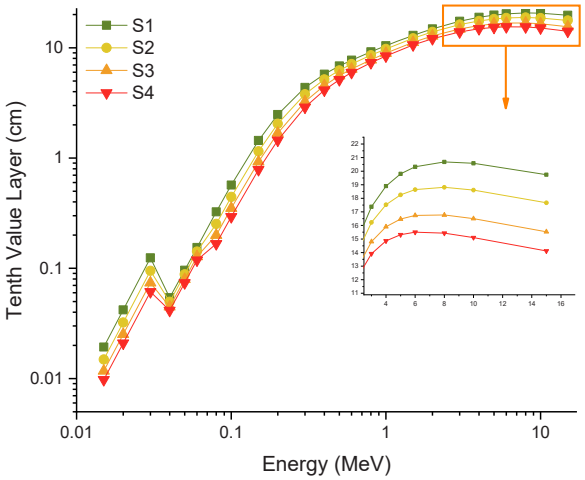

Fig. 8. Variation of tenth value layer (cm) with photon energy (MeV) for all S1-S4 glasses.

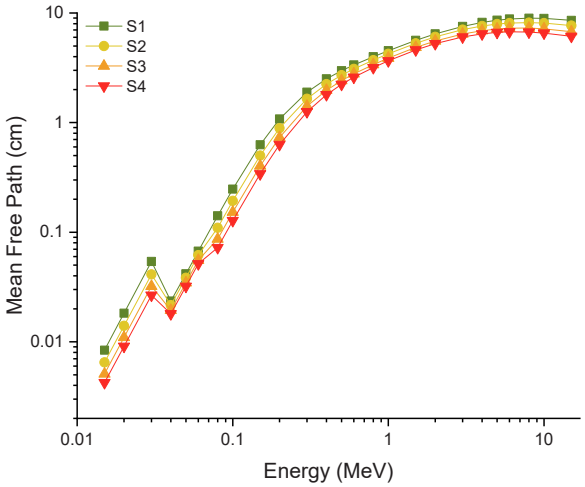

Fig. 9. Variations of mean free path (cm) with photon energy (MeV) for all S1-S4 glasses.

shows the linear attenuation coefficient's evolution with respect to various energy values. Depending on the photon's energy, a variety of interactions may take place when it comes into contact with matter [46–49]. The photoelectric effect (PE), for example, is the most common type interaction in the lower energy band. This is evident in Fig. 5, which shows a fast drop in linear attenuation coefficients in the low-energy area. We noticed that the linear attenuation coefficients of the S4 sample were the highest of all the glass materials tested. The additive's indirect effect on glass density and the maximum WO_3 contribution both play a role in this situation. After that, we calculated the density-independent crucial gamma-ray shielding parameter namely mass attenuation coefficients (μ_m). With increasing photon energy (MeV), mass attenuation coefficients (cm^2/g) for all S1-S4 glasses vary. Over a wide range of gamma-ray energies, we noticed similar characteristics, such as linear attenuation coefficients. S4 had the highest mass attenuation coefficients of all of the glasses tested, however. There's a possibility that the larger atomic number of WO_3 at S4's maximum concentration influenced the behavior of mass attenuation coefficients. Half value layer (HVL) is the thickness of the shielding material that reduces the gamma radiation's intensity by half. As a result, materials with better gamma-ray shielding properties are those that can reduce their intensity by half at thinner thicknesses. The HVL values of the glass samples utilized in this study were obtained using an energy range of 0.015–15 MeV. Fig. 7 shows the gamma-ray energy values for samples S1, S2, S3, and S4 in relation to their HVL values. According to the results shown, the glass samples' behaviors changed dramatically as the thickness of the half-value layer rose. For example, in the low-energy zone, half-value thicknesses are the lowest, but as energy increases, they expand in proportion. Low-energy photons have weak penetrating abilities, which reduces their intensity by a factor of two when travelling through extremely thin materials. Because of their density and weight, all glass samples investigated had a relatively modest HVL thickness for the low energy zone. Thickness values in the high energy zone reached 3–4 cm, as seen in the graph. Using Fig. 7, we can observe that the S4 sample has the lowest HVL values over the entire energy range. With respect to a particular radiation intensity, the attenuation coefficients of the S4 sample lead to an understanding of its ability to achieve the thinnest potential half-value thickness among all of the glass

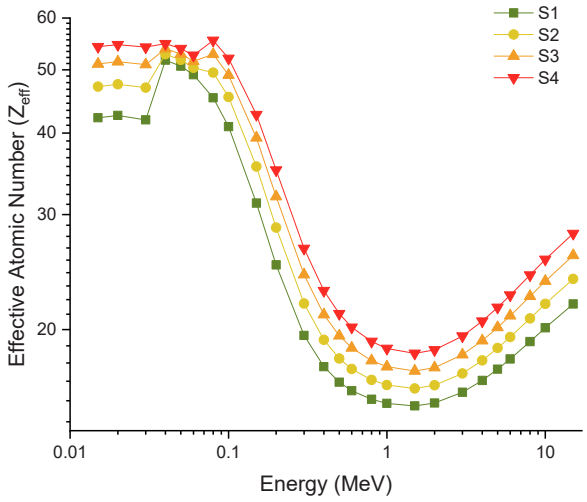

Fig. 10. Variations of effective atomic number (Z_{eff}) with photon energy (MeV) for all S1-S4 glasses.

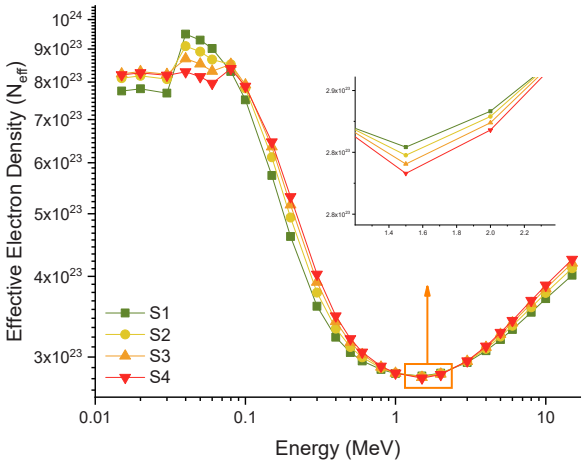

Fig. 11. Variations of effective electron density (electrons/g) with photon energy (MeV) for all S1-S4 glasses.

samples tested. As an alternative, the TVL may be used to determine another fundamental shielding component that is identical to the half-value layer and offers the same operational information. This value, like the HVL, describes the thickness of the material needed to reduce the radiation intensity of the material by 10%. Fig. 8 shows how the thickness of one tenth of the tested heavy metal oxide glasses changes as a function of energy. Compared to half-value layer values, tenth-value layer values have bigger quantitative values for the same energy levels. This is an inherent occurrence to observe higher shielding material thicknesses are needed to reduce the intensity of radiation with a specific energy value by one tenth of its original value. Quantitatively, however, the S4 sample has the lowest one-tenth value thickness values for each of these properties, even when comparing the identical energy values. S4 provides half and tenth value thicknesses in processes with photon energies ranging from 0.015 to 15 MeV when these two important properties are taken into consideration. Thus, the S4 sample is the most cost-effective and takes up the least amount of space when compared to the other glass samples. Interactions between a single photon and the material occur within the material after the radiation first contacts the absorber layer and penetrates into the background. When the energy of the incoming radiation is lowered to zero, the radiation is completely absorbed. With the mfp parameter, we may choose how far apart two photon interactions inside a material should be. Investigators may use this tool to assess how modifications in doping and chemical composition impact the subsequent interaction length, which is critical for comparison-based studies. All S1-S4 glasses' mean free path (cm) changes as a function of photon energy (MeV) are shown in Fig. 9. Clearly, Fig. 9 shows that gamma ray penetrating characteristics are linked to the gamma ray's mean travel distance. As the energy of gamma rays increased, the mean free component values increased as well. However, the S4 sample exhibited the lowest mean free path values of all of the gamma ray energies. Fig. 10 depicts the relationship between the photon energy and the effective atomic number (Z_{eff}) (MeV). In the low-energy zone, photoelectric-interaction was most prevalent, hence Z_{eff} values were highest. The glass matrix's greater Z (W=74) increased Z_{eff} significantly in the lowest energy range. Because of the high frequency of

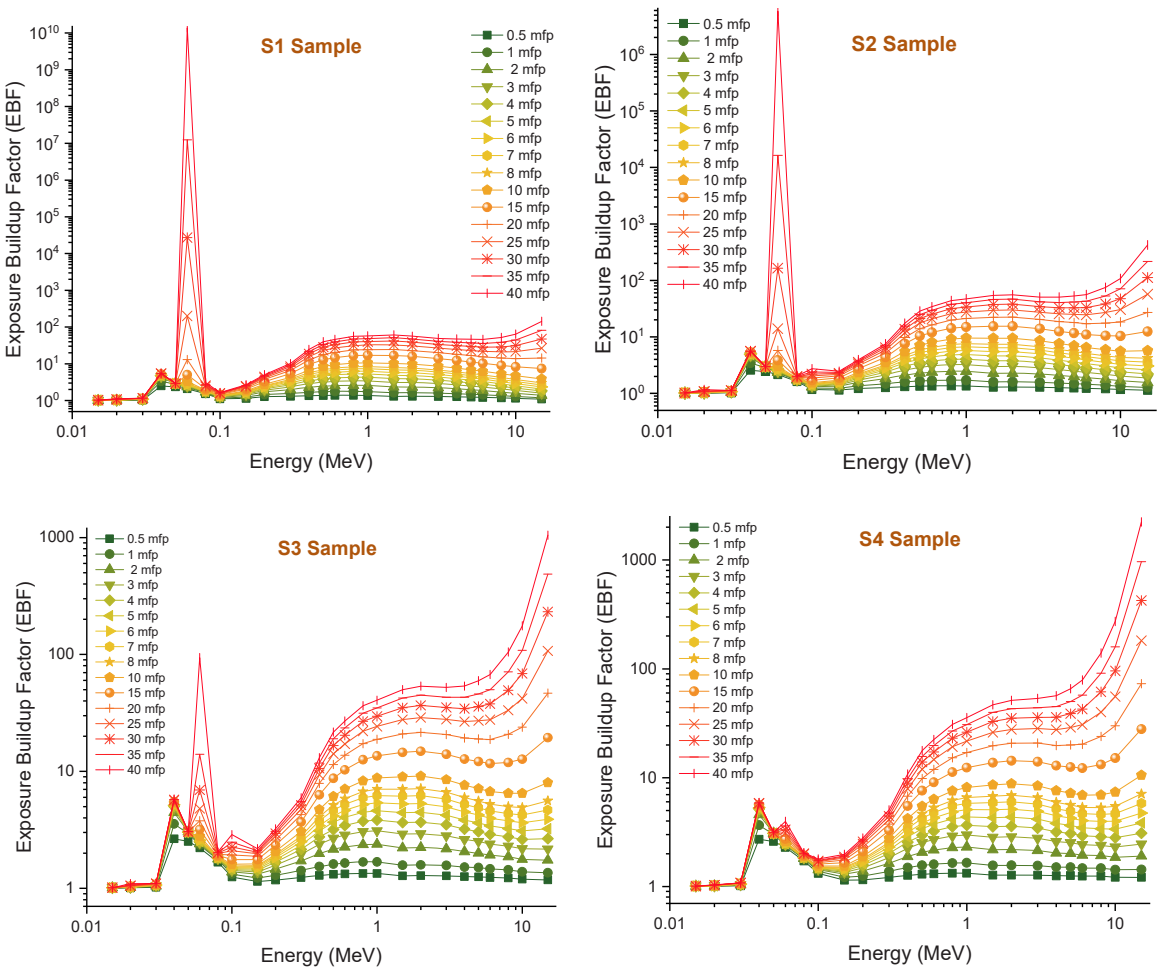

Fig. 12. : Variation of exposure buildup factors (EBF) of investigated glasses at different mean free path values.

Compton scattering, the Zeff values in the intermediate energy band decreased significantly. This clearly shows that the maximum possible Z_{eff} values for the photon energy are found in the S4 with the highest mass attenuation coefficients. The effective electron density (N_{eff}) is directly related to the effective atomic number (Z_{eff}). The N_{eff} values of glasses S1 through S4 were determined utilizing a compound concept for multi-element glass samples. As shown in Fig. 11, the photon energy (MeV) influences the change in effective electron density (electrons/g) for all S1-S4 glasses. The N_{eff} values, when compared to the Z_{eff} values, exhibit a similar energy-dependent trend. The findings indicated that the S4 sample, which had the greatest effective atomic number, also possessed the highest effective electron density, implying a relationship between these two measures. The term build-up factor is a very important term in terms of materials engineering, which is generally used to understand the contribution of photons that interact and do not interact during the absorption process to the total absorption process. The build-up factor is also crucial in medical radiation protection devices to better understand how the material interacts with incoming gamma rays. The build-up factor term may be divided into two primary categories: exposure (EBF) and energy absorption (EABF) build-up factor values. Using gamma-ray energy (MeV) as a variable, the EBF and EABF dispersion along different mean free routes are shown in Figs. 12 and 13, respectively. Due to photoelectric absorption, which absorbs the majority of incoming gamma rays, we discovered low EBF and EABF values in the low gamma-ray energy range. At around 0.1 MeV, however, the EBF and EABF values quickly increase as Compton Scattering becomes significant. According to our findings, increasing the amount of WO_3 reinforcement decreased EBF and EABF values across the board (i.e., from 0.5 to 40 mfp). When W increases from S1 to S4, the collision rate of incoming gamma rays with glass samples increases significantly. Finally, gamma-ray transmission factor (TF) values were calculated for S1, S2, S3, S4 glass samples for a range of well-known radioisotope energies (see Table 2) emitted from ^{67}Ga, ^{57}Co-57, ^{111}In-111, ^{133}Ba, ^{201}Tl, $^{99\,m}$Tc, ^{51}Cr, ^{131}I, ^{58}Co, ^{137}Cs, ^{60}Co. The TF values of the glasses under examination were derived using two separate approaches. In Fig. 14, the TFs of the investigated glasses are shown against the radioisotope energy (MeV) employed at various glass thicknesses. As radioisotope energy increases, the predicted transmission factor increases as well (i.e., from 0.0086 MeV to 1.3326 MeV). To begin, we discovered that glass samples of all thicknesses exhibited the lowest TF values in the low-energy zone. This is because these dense samples have a large capacity for attenuating low-energy gamma-rays. Nonetheless, there seems to be a considerable divergence at 0.1 MeV. After 0.1 MeV, glass

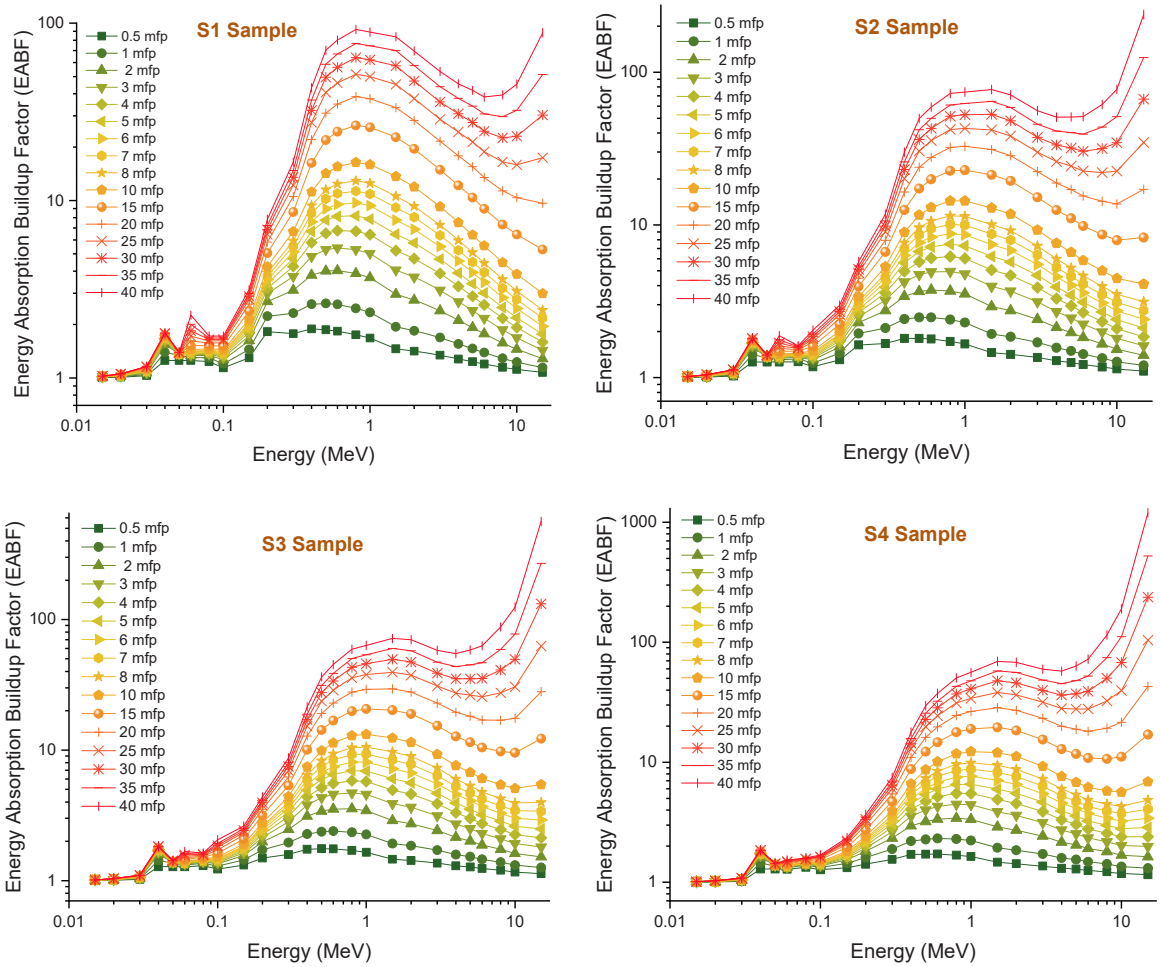

Fig. 13. : Variation of energy absorption buildup factors (EABF) of investigated glasses at different mean free path values.

Table 2
Radioisotopes and gamma-ray energies used for gamma-ray TF calculations.

Radioisotope	Gamma-ray energy (MeV)
^{67}Ga	0.0086, 0.0093, 0.1840
^{57}Co	0.0144, 0.1221, 0.1365
^{111}In	0.0230, 0.1710, 0.2450
^{133}Ba	0.0532, 0.0796, 0.0810, 0.2764, 0.3029, 0.3560, 0.3838
^{201}Tl	0.0710, 0.1350, 0.1670
$^{99\ m}$Tc	0.1405
^{51}Cr	0.3201
^{131}I	0.2843, 0.3645, 0.6370, 0.7229
^{58}Co	0.5110, 0.8108
^{137}Cs	0.6617
^{60}Co	1.1732, 1.3325

samples of varied thickness exhibit a spectrum of gamma ray reactions. The highest self-absorption values were established for all glass samples examined at a thickness of 3 cm. This is because shield thickness influences the attenuation capacity of any shielding material, suggesting that increasing shield thickness enhances the attenuation capacity of incoming gamma rays. Following that, we thoroughly studied the TF values of the investigated glasses by comparing their attenuation capabilities for glass thicknesses of 0.5 cm. The Transmission Factors (TFs) of different glass thicknesses are shown against the radioisotope energy (MeV) used in Fig. 15. When can be seen, as the incoming gamma-ray energy rises, the TF values fall throughout all thicknesses. However, across all glass thicknesses investigated, the S4 sample exhibited good transmission qualities against powerful gamma-rays. In the final phase of the study, the HVL values of the S4 sample, which showed superior gamma ray absorption properties, were compared with many glass and concrete

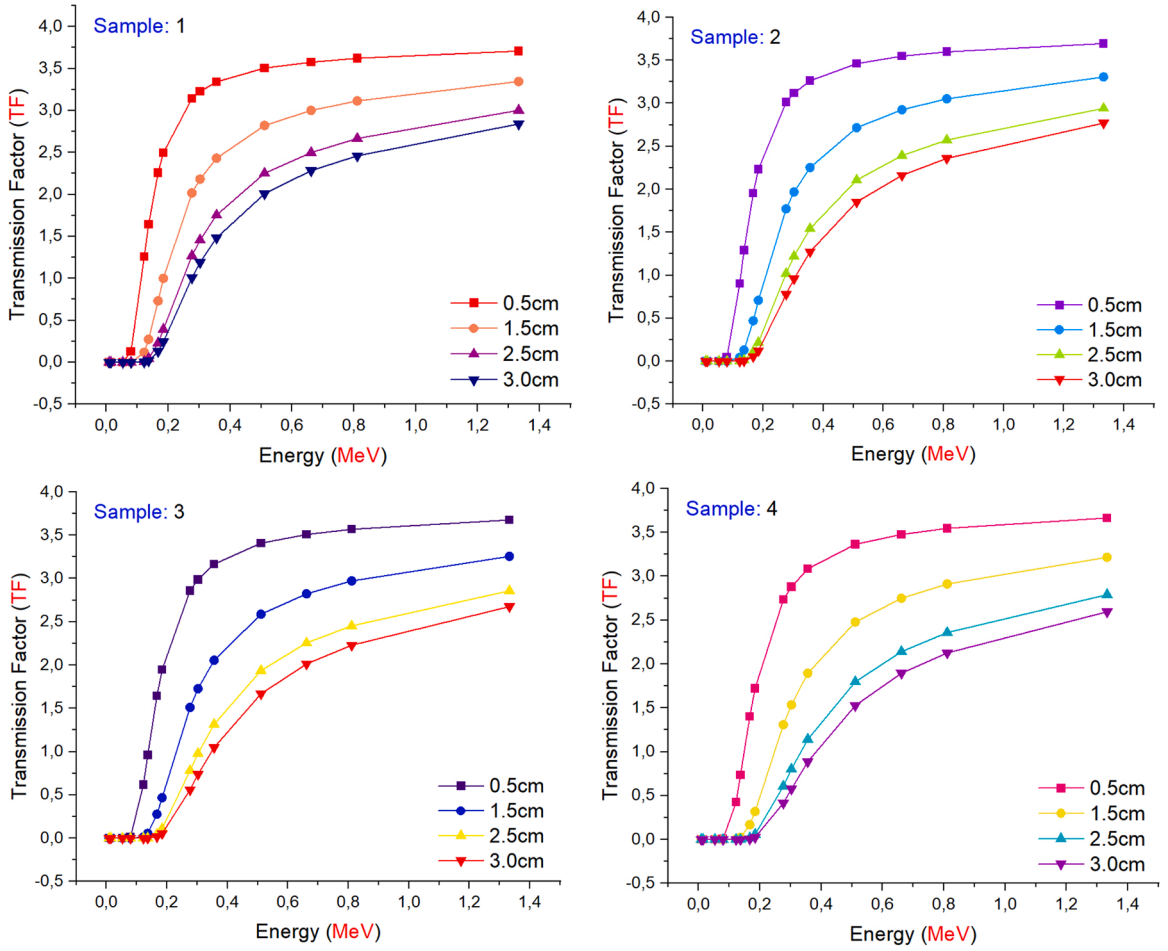

Fig. 14. : Transmission Factors (TFs) of investigated glasses as a function of used radioisotope energy (MeV) at different glass thicknesses.

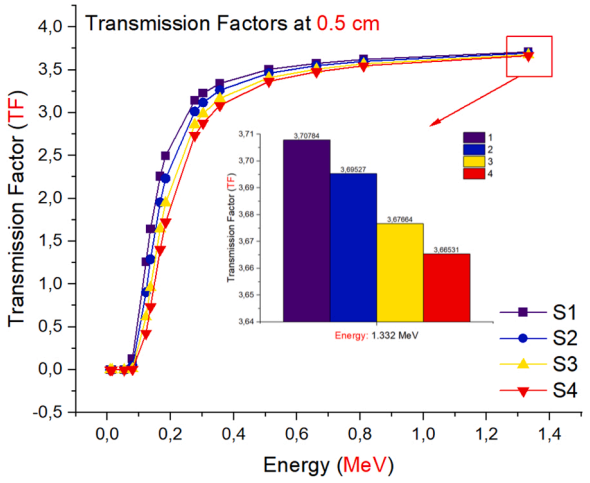

Fig. 15. : Comparison of the Transmission Factors (TFs) as a function of used radioisotope energy (MeV) for different glass thicknesses.

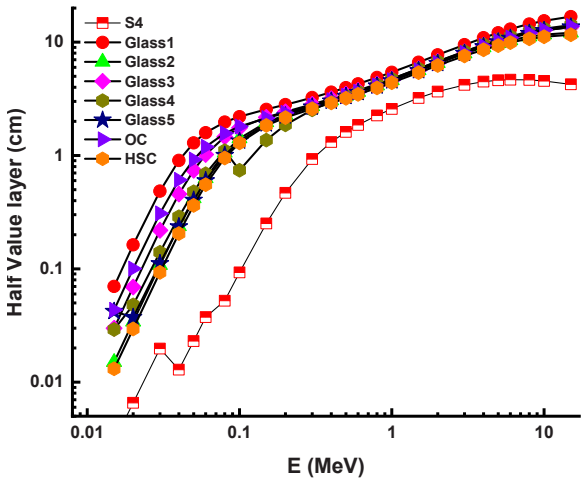

Fig. 16. Comparison of HVL values for other glass shields and concrete shields.

shielding materials available in the literature in a wide energy range. Other shielding materials used for HVL comparison are listed as follows.

- Glass1 [50]
- Glass2 [51]
- Glass3 [52]
- Glass4 [53]
- Glass5 [54]
- Ordinary Concrete (OC) and Hematite-Serpentine Concrete (HSC) [55]

Fig. 16 depicts the comparison of HVL values for other glass shields and concrete shields in 0.015–15 MeV photon energy range. As can be seen from the figure, the of the HVL behaviours of the compared materials as a function of the energy values are similar for all materials. For example, the lowest quantitative values of HVL values in the low energy region indicate that the required thickness by all materials for low energy gamma rays are low. However, it is seen that the HVL values increase with the increase in the gamma ray energy values, and the maximum HVL values were observed in the high energy region for all shielding materials. This behavioural tendency is an expected situation for all candidate shielding materials, and as mentioned in the previous sections, shielding material that provides a lower HVL value for the same energy value is considered superior. As can be seen from the figure, the HVL values provided by the S4 sample have the lowest quantitative values among all the compared materials in the low, medium, and high energy regions. It is clearly seen that the S4 sample shows much lower HVL values, especially in the 0.015–1 MeV range. This indicates that the S4 sample may be a more advantageous sample if used for medical radioisotopes existing in the relevant range and considered as part of this study.

4. Conclusion

Using Makishima-Mackenzie model, the mechanical properties of barium-phosphate-tungsten oxides with chemical formula (50-x) P_2O_5-50BaO-xWO_3 (x = 0.0(S1), 5.0(S2), 10(S3), and 15(S4)) mole% was evaluated. As well as the newly online Phy-X/PSD software and Monte Carlo code were used to examine the gamma radiation attenuation characteristics. Our findings.

revealed that: The total packing density (V_t) was enhanced from 0.589 for S1 glass sample (free with WO_3) to 0.605 for S4 glass sample (with highest WO_3 =15 mol%). The total energy dissociation (G_t) of the investigated glasses were increased with increasing the WO_3 content: from 51.7 (kJ/cm^3) for S1 glasses to 52.45 (kJ/cm^3) for S4 glasses. All mechanical moduli (Young's, shear, bulk, and longitudinal) moduli were improved with increasing the tungsten trioxide concentration in the studied glasses. Poisson's ratios were increased with increasing the WO_3 concentration in the studied glasses. At the conclusion of the study, it was determined that increasing the WO3 additive had a direct influence on the gamma ray absorption capabilities. For example, the S1 sample with the lowest WO3 contribution had the lowest LAC, MAC, and maximum HVL values, while the S4 sample with the greatest WO3 contribution had the highest LAC, MAC, and minimum HVL values. This behavioral tendency, which was observed in the energy range of 0.015–15 MeV, corresponded with the energies of many industrial and medicinal radioisotopes. The comparison to other glass and concrete shielding materials in the literature revealed that the S4 sample with the greatest WO3 addition outperformed many glassy structures and, more crucially, shielding concretes that had previously been shown with better qualities. One of the most significant implications to be derived from these findings is that S4 and comparable glass shielding materials may be one of the most viable choices for medical and industrial radiation areas that employ conventional concrete and reinforced concrete. Consequently, this

research is a continuation of a previously published work, and glass samples were modeled and studied based on their chemical composition. Additionally, experimental examination and testing of these materials with medical radiation sources in clinical regions is recommended.

Funding

Princess Nourah bint Abdul Rahman University Researchers Supporting Project Number (PNURSP2022R149).

Declaration of Competing Interest

There are no conflicts of interest to declare.

Data Availability

Data will be made available on request.

Acknowledgement

This work was performed under Princess Nourah bint Abdulrahman University Researchers Supporting Project Number (PNURSP2022R149), Princess Nourah bint Abdulrahman University, Riyadh, Saudi Arabia. Authors express their sincere gratitude to Princess Nourah bint Abdulrahman University.

References

[1] D.D. Rao, Summary from the SFRP-IRPA workshops “on the reasonableness in the practical implementation of the ALARA principle, Radiat. Prot. Environ. 42 (4) (2019) 187.
[2] G. Lakshminarayana, S.O. Baki, K.M. Kaky, M.I. Sayyed, H.O. Tekin, A. Lira, I.V. Kityk, M.A. Mahdi, Investigation of structural, thermal properties and shielding parameters for multicomponent borate glasses for gamma and neutron radiation shielding applications, J. Non-Cryst. Solids 471 (2017) 222–237.
[3] M. Haghparast, R. Afzalipour, S. Ahmadi, M.S. GolverdiYazdi, K. DindarlooInaloo, M. Saanei, Quality control of radiology devices in Health Centers Affiliated with Hormozgan University of Medical Sciences, Bimon. J. Hormozgan Univ. Med. Sci. 19 (1) (2015) 46–52.
[4] G.J. Scuderi, G.V. Brusovanik, D.R. Campbell, R.P. Henry, B. Kwon, A.R. Vaccaro, Evaluation of non–lead-based protective radiological material in spinal surgery, Spine J. 6 (5) (2006) 577–582.
[5] H. Mori, K. Koshida, O. Ishigamori, K. Matsubara, Evaluation of the effectiveness of X-ray protective aprons in experimental and practical fields, Radiol. Phys. Technol. 7 (1) (2014) 158–166.
[6] U. Kara, G. Susoy, S.A. Issa, W. Elshami, N.Y. Yorgun, M.M. Abuzaid, E. Kavaz, H.O. Tekin, Scanning electron microscopy (SEM), energy-dispersive X-ray (EDX) spectroscopy and nuclear radiation shielding properties of [α-Fe3+O(OH)]-doped lithium borate glasses, Appl. Phys. A 126 (7) (2020) 1–14.
[7] M.M. Abuzaid, G. Susoy, S.A. Issa, W. Elshami, O. Kilicoglu, H.O. Tekin, Relationship between melting-conditions and gamma shielding performance of fluoro-sulfo-phosphate (FPS) glass systems: a comparative investigation, Ceram. Int. 46 (10) (2020) 15255–15269.
[8] Y.B. Saddeek, H.O. Tekin, S.A. Issa, O. Kilicoglu, W. Elshami, T. Alharbi, An in-depth investigation from mechanical durability to structural and nuclear radiation attenuation properties: B2O3–Na2O–Bi2O3–Nb2O5 glasses experience, Phys. Scr. 95 (10) (2020), 105701.
[9] E. Kavaz, F.I. El_Agawany, H.O. Tekin, U. Perişanoğlu, Y.S. Rammah, Nuclear radiation shielding using barium borosilicate glass ceramics, J. Phys. Chem. Solids 142 (2020), 109437.
[10] N. Singh, K.J. Singh, K. Singh, H. Singh, Comparative study of lead borate and bismuth lead borate glass systems as gamma-radiation shielding materials, Nucl. Instrum. Methods Phys. Res. Sect. B Beam Interact. Mater. At. 225 (2004) 305–309.
[11] V.P. Singh, N.M. Badiger, N. Chanthima, J. Kaewkhao, Evaluation of gamma-ray exposure buildup factors and neutron shielding for bismuth borosilicate glasses, Radiat. Phys. Chem. 98 (2014) 14–21.
[12] H.O. Tekin, Shams A.M. Issa, Emad M. Ahmed, Y.S. Rammah, Lithium-fluoro borotellurite glasses: nonlinear optical, mechanical, characteristics and gamma radiation protection characteristics, Radiat. Phys. Chem. 190 (2022), 109819, https://doi.org/10.1016/j.radphyschem.2021.109819.
[13] H.A. Saudi, Hesham M.H. Zakaly, Shams A.M. Issa, H.O. Tekin, M.M. Hessien, Y.S. Rammah, A.M.A. Henaish, Fabrication, FTIR, physical characteristics and photon shielding efficacy of CeO2 /sand reinforced borate glasses: experimental and simulation studies, Radiat. Phys. Chem. 191 (2022), 109837, https://doi.org/10.1016/j.radphyschem.2021.109837.
[14] A.S. Abouhaswa, F.I. El-Agawany, Emad M. Ahmed, Y.S. Rammah, Optical, magnetic characteristics, and nuclear radiation shielding capacity of newly synthesized barium boro-vanadate glasses: B2O3–BaF2–Na2O–V2O5, Radiat. Phys. Chem. 192 (2022), 109922, https://doi.org/10.1016/j.radphyschem.2021.109922.
[15] N. Ekinci, F.I. El-Agawany, A. Gurol, Y.S. Rammah, Emad M. Ahmed, D. Yılmaz, Bunyamin Aygün, M. Somer, Physical properties, experimental and theoretical gamma-ray shielding properties of some boron compounds, Radiat. Phys. Chem. 194 (2022), 110012, https://doi.org/10.1016/j.radphyschem.2022.110012.
[16] Aylin M. Deliormanlı, Mertcan Ensoylu, Shams A.M. Issa, Y.S. Rammah, Ghada ALMisned, H.O. Tekin, A thorough examination of gadolinium (III)-containing silicate bioactive glasses: synthesis, physical, mechanical, elastic and radiation attenuation properties, Appl. Phys. A 128 (2022) 266, https://doi.org/10.1007/s00339-022-05408-0.
[17] H.H. Somaily, H. Algarni, Y.S. Rammah, Amani Alalawi, C. Mutuwong, M.S. Al-Buriahi, The effects of V2O5/K2O substitution on linear and nonlinear optical properties and the gamma ray shielding performance of TVK glasses, Ceram. Int. 47 (2021) 1012–1020, https://doi.org/10.1016/j.ceramint.2020.08.215.
[18] M.I. Sayyed, Y. Al-Hadeethi, Maha M. AlShammari, Moustafa Ahmed, Saleh H. Al-Heniti, Y.S. Rammah, Physical, optical and gamma radiation shielding competence of newly boro-tellurite based glasses: TeO2 –B2O3 –ZnO–Li2O3 –Bi2O3, Ceram. Int. 47 (2021) 611–618, https://doi.org/10.1016/j.ceramint.2020.08.168.
[19] Y.S. Rammah, I.O. Olarinoye, F.I. El-Agawany, A. El-Adawy, El. Sayed Yousef, The impact of PbF2 on the ionizing radiation shielding competence and mechanical properties of TeO2–PbF2 glasses and glass-ceramics, Ceram. Int. 47 (2021) 2547–2556, https://doi.org/10.1016/j.ceramint.2020.09.100.
[20] H.H. Hegazy, M.S. Al-Buriahi, Faisal Alresheedi, F.I. El-Agawany, Chahkrit Sriwunkum, R. Neffati, Y.S. Rammah, Nuclear shielding properties of B2O3–Bi2O3–SrO glasses modified with Nd2O3: Theoretical and simulation studies, Ceram. Int. 47 (2021) 2772–2780, https://doi.org/10.1016/j.ceramint.2020.09.131.
[21] Y.S. Rammah, F.I. El-Agawany, N. Elkhoshkhany, F. Elmasry, M. Reben, Iwona Grelowska, E. Yousef, Physical, optical, thermal, and gamma-ray shielding features of fluorotellurite lithiumniobate glasses: TeO2-LiNbO3-BaO-BaF2-La2O3, J. Mater. Sci: Mater. Electron 32 (2021) 3743–3752, https://doi.org/10.1007/s10854-020-05119-3.

[22] M.S. Shams, Samir Y. Marzouk, Adel M. El-Refaey, Shams H. Abdel-Hafez, I.O. Olarinoye, Y.S. Rammah, J. Mater. Res. Tech. 15 (2021) 5540–5553, https://doi.org/10.1016/j.jmrt.2021.10.134.

[23] H.M.H. Zakaly, A. Ene, I.O. Olarinoye, S.Y. Marzouk, S.H. Abdel-Hafez, M.S. Shams, Y.S. Rammah, Investigation of Er3+ ions reinforced zinc-phosphate glasses for ionizing radiation shielding applications, Materials 14 (2021) 6769, https://doi.org/10.3390/ma14226769.

[24] G. ALMisned, W. Elshami, Shams A.M. Issa, G. Susoy, Hesham M.H. Zakaly, M. Algethami, Y.S. Rammah, A. Ene, S.A. Al-Ghamdi, A.A. Ibraheem, H.O. Tekin, Enhancement of gamma-ray shielding properties in cobalt-doped heavy metal borate glasses: the role of lanthanum oxide reinforcement, Materials 14 (2021) 7703, https://doi.org/10.3390/ma14247703.

[25] RSICC Computer Code Collection, MCNPX User's Manual Version 2.4.0. Monte Carlo N-Particle Transport Code System for Multiple and High Energy Applications; 2002.

[26] E. Şakar, Ö.F. Özpolat, B. Alım, M.I. Sayyed, M. Kurudirek, Phy-X/PSD: development of a user friendly online software for calculation of parameters relevant to radiation shielding and dosimetry, Radiat. Phys. Chem. 166 (2020), 108496, https://doi.org/10.1016/j.radphyschem.2019.108496.

[27] Y. Al-Hadeethi, M.I. Sayyed, Y.S. Rammah, Fabrication, optical, structural and gamma radiation shielding characterizations of GeO2-PbO-Al2O3–CaO glasses, Ceram. Int. 46 (2020) 2055–2062, https://doi.org/10.1016/j.ceramint.2019.09.185.

[28] M.S. Al-Buriahi, F.I. El-Agawany, C. Sriwunkum, Hakan Akyıldırım, Halil Arslan, B.T. Tonguc, R. El-Mallawany, Y.S. Rammah, Influence of Bi2O3/PbO on nuclear shielding characteristics of lead-zinc-tellurite glasses, Phys. B 581 (2020), 411946, https://doi.org/10.1016/j.physb.2019.411946.

[29] F.I. El-Agawany, O.L. Tashlykov, K.A. Mahmoud, Y.S. Rammah, The radiation-shielding properties of ternary SiO2–SnO–SnF2 glasses: simulation and theoretical study, Ceram. Int. 46 (2020) 23369–23378, https://doi.org/10.1016/j.ceramint.2020.04.042.

[30] Gokhan Kilic, Erkan Ilik, K.A. Mahmoud, R. El-Mallawany, F.I. El-Agawany, Y.S. Rammah, Novel zinc vanadyl boro-phosphate glasses: ZnO–V2O5– P2O5 –B2O3: physical, thermal, and nuclear radiation shielding properties, Ceram. Int. 46 (2020) 19318–19327.

[31] Petr Kalenda, Ladislav Koudelka, Petr Mośner, Lionel Montagne, Bertrand Revel, Glass-forming ability and the structure of glasses in the BaO-WO3-P2O5 system, J. Non-Cryst. Solids 541 (2020), 120145.

[32] A. Makishima, J.D. Mackenzie, Direct calculation of Young's modulus of glass, J. Non-Cryst. Solids 12 (1) (1973) 35–45 (1973).

[33] S. Inaba, Sh Fujino, K. Morinaga, Young's modulus and compositional parameters of oxide glasses, J. Am. Ceram. Soc. 82 (12) (1999) 3501–3507 (1999).

[34] I.O. Olarinoye, F.I. El-Agawany, A. El-Adawy, El-Sayed Yousef, Y.S. Rammah, Mechanical features, alpha particles, photon, proton, and neutron interaction parameters of TeO2–V2O3–MoO3 semiconductor glasses, Ceram. Int. 46 (2020) 23134–23144.

[35] Y.S. Rammah, I.O. Olarinoye, F.I. El-Agawany, A. El-Adawy, A. Gamal, El Sayed Yousef., Elastic moduli, photon, neutron, and proton shielding parameters of tellurite bismo-vanadate (TeO2–V2O5–Bi2O3) semiconductor glasses, Ceram. Int. 46 (2020) 25440–25452.

[36] N. Elkhoshkhany, E. Syala, E. Yousef, Concentration dependence of the elastic moduli, thermal properties, and non-isothermal kinetic parameters of Yb3+ doped multicomponent tellurite glass system, Results Phys. 16 (2020), 102876.

[37] M. Almateri, O. Agar, E.E. Altunsoy, O. Kilicoglu, M.I. Sayyed, H.O. Tekin, Photon and neutron shielding characteristics of samarium doped lead alumino borate glasses containing barium, lithium and zinc oxides determined at medical diagnostic energies, Results Phys. 12 (2019) 2123–2128, https://doi.org/10.1016/j.rinp.2019.01.094.

[38] C.C. de Araujo, W. Strojek, L. Zhang, H. Eckert, G. Poirier, S.J.L. Ribeiro, Y. Messaddeq, Structural studies of $NaPO_3$ -WO_3 glasses by solid state NMR and Raman, Spectrosc. J. Mater. Chem. 16 (2006) 3277–3284.

[39] T. Sekiya, N. Mochida, S. Ogawa, Structural study of WO_3 -TeO_2 glasses, J. Non-Cryst. Solids 176 (1994) 105–115.

[40] D.R. Lide, Handbook of Chemistry and Physics, CRC Press, Boca Raton, 2001, pp. 9–52.

[41] S. Inaba, S. Oda, K. Morinaga, Heat capacity of oxide glasses at high temperature region, J. Non-Cryst. Solids 325 (2003) 258–266.

[42] F.Z. Agti, M.T. Soltani, L.F. Santos, A. Messaoudi, N. Guesmia, D.D. Ligny, Physical, mechanical properties and optical dispersion in Sb_2O_3–$NaPO_3$-WO_3 glasses, J. Non-Cryst. Solids 576 (2022), 121249.

[43] T. Rouxel, Elastic properties and short-to medium-range order in glasses, J. Am. Ceram. Soc. 90 (2007) 3019–3039, https://doi.org/10.1111/j.1551-2916.2007.01945.x.

[44] S. Azianty, A.K. Yahya, Enhancement of elastic properties by WO_3 partial replacement of TeO_2 in ternary (80 − x)TeO_2–20PbO–xWO_3 glass system, J. Non-Cryst. Solids 378 (2013) 234–240, https://doi.org/10.1016/j.jnoncrysol.2013.07.016.

[45] El. Sayed Yousef, Amin El-Adawy, N. El Koshkhany, E.R. Shaaban, Optical and acoustic properties of TeO_2/WO_3 glasses with small amount of additive ZrO_2, J. Phys. Chem. Solids 67 (2006) 1649–1655.

[46] H.O. Tekin, Ghada ALMisned, Hesham M.H. Zakaly, Abdallah Zamil, Dalia Khoucheich, Ghaida Bilal, Lubna Al-Sammarraie, Shams A.M. Issa, Mohammed Sultan Al-Buriahi, Antoaneta Ene, Gamma, neutron, and heavy charged ion shielding properties of Er3+-doped and Sm3+- doped zinc borate glasses, Open Chem. 20 (2022) 130–145, https://doi.org/10.1515/chem-2022-0128.

[47] H.O. Tekin, Ghada ALMisned, Gulfem Susoy, Fatema T. Ali, Duygu Sen Baykal, Antoaneta Ene, Shams A.M. Issa, Yasser S. Rammah, Hesham M.H. Zakaly, Transmission factor (TF) behavior of Bi2O3–TeO2–Na2O–TiO2–ZnO glass system: a monte carlo simulation study, Sustainability 14 (2022) 2893, https://doi.org/10.3390/su14052893.

[48] G. Lakshminarayana, Ashok Kumar, H.O. Tekin, Shams A.M. Issa, M.S. Al-Buriahi, M.G. Dong, Dong-Eun Lee, Jonghun Yoon, Taejoon Park, Illustration of distinct nuclear radiation transmission factors combined with physical and elastic characteristics of barium boro-bismuthate glasses, Results Phys. (2021), 105067, https://doi.org/10.1016/j.rinp.2021.105067.

[49] Y.S. Rammah, Influence of Ag2O insertion on alpha, proton and γ-rays safety features of TeO2.ZnO.Na2O glasses: potential use for nuclear medicine applications, Ceram. Int. 46 (2020) 18151–18159, https://doi.org/10.1016/j.ceramint.2020.04.136.

[50] B. Aktas, S. Yalcin, K. Dogru, Z. Uzunoglu, D. Yilmaz, Structural and radiation shielding properties of chromium oxide doped borosilicate glass, Radiat. Phys. Chem. 156 (2019) 144–149, https://doi.org/10.1016/j.radphyschem.2018.11.012.

[51] S. Yalcin, B. Aktas, D. Yilmaz, Radiation shielding properties of cerium oxide and erbium oxide doped obsidian glass, Radiat. Phys. Chem. 160 (2019) 83–88, https://doi.org/10.1016/j.radphyschem.2019.03.024.

[52] Haifa A. Al-Yousef, M.I. Sayyed, Mohammed Alotiby, Ashok Kumar, Yasser S. Alghamdi, B.M. Alotaibi, Norah A.M. Alsaif, K.A. Mahmoud, Y. Al-Hadeethi, Evaluation of optical, and radiation shielding features of new phosphate-based glass system, Optik 242 (2021), 167220, https://doi.org/10.1016/j.ijleo.2021.167220.

[53] Aljawhara H. Almuqrin, Ashok Kumar, J.F.M. Jecong, Nuha Al-Harbi, E. Hannachi, M.I. Sayyed, Li2O-K2O-B2O3-PbO glass system: optical and gamma-ray shielding investigations, Optik 247 (2021), 167792, https://doi.org/10.1016/j.ijleo.2021.167792.

[54] Fatemah Farraj Al-Harbi, Nimitha S. Prabhu, M.I. Sayyed, Aljawhara H. Almuqrin, Ashok Kumar, Sudha D. Kamath, Evaluation of structural and gamma ray shielding competence of Li2O-K2O-B2O3-HMO (HMO = SrO/TeO2/PbO/Bi2O3) glass system, Optik 248 (2021), 168074, https://doi.org/10.1016/j.ijleo.2021.168074.

[55] I.I. Bashter, Calculation of radiation attenuation coefficients for shielding concretes, Ann. Nucl. Energy 24 (1997) 1389–1401, https://doi.org/10.1016/S0306-4549(97)00003-0.